CrossMark

Hyperthermia studies using inductive and ultrasound methods on *E. coli* bacteria and mouse glioma cells

A. Cabral–Prieto[1] (iD) **· R. López-Callejas[1] · B. G. Rodríguez-Méndez[1] · C. L. Santos-Cuevas[1] · J. Celis-Almazán[2] · O. Olea-Mejía[2] · J. L. Gómez-Morales[3] · R. Peña-Eguiluz[1] · R. Valencia-Alvarado[1] · A. Mercado-Cabrera[1] · A. E. Muñoz-Castro[1] · F. García-Santibañez[3]**

Abstract The survival of *Escherichia coli* bacteria and *mouse glioma* cells were studied under different temperatures using direct heating in water, ultrasound, and magnetic fluid hyperthermia. The survival of these microorganisms depended on whether the heating mode

✉ A. Cabral–Prieto
  agustin.cabral@inin.gob.mx

  R. López-Callejas
  regulo.lopez@inin.gob.mx

  B. G. Rodríguez-Méndez
  benjamin.rodriguez@inin.gob.mx

  C. L. Santos-Cuevas
  clara.cuevas@inin.gob.mx

  J. Celis-Almazán
  jony_jac_5@hotmail.com

  O. Olea-Mejía
  oleaoscar@yahoo.com.mx

  R. Peña-Eguiluz
  rosendo.eguiluz@inin.gob.mx

  R. Valencia-Alvarado
  raul.valencia@inin.gob.mx

  A. Mercado-Cabrera
  antonio.mercado@inin.gob.mx

  A. E. Muñoz-Castro
  arturo.munoz@inin.gob.mx

  F. García-Santibañez
  fegasa2@yahoo.com.mx

🙌 Springer

was continuous or discontinuous, surviving more in the former than in the discontinuous heating mode. Whereas *Escherichia coli* bacteria did not survive at temperatures $\geq 50°C$, the *mouse glioma* cells did not survive at temperatures $\geq 48°C$. The survival of both these microorganisms was independent of the presence or absence of the magnetic nanoparticles of magnetite, suggesting that these, having mean particle sizes of 9.5, 8.5 and 5, did not show any apparent cytotoxicity effect. Present results also showed that the inductive heating system which used a radiofrequency of 13.56 MHz, providing a maximum magnetic field strength of 160 A/m, the electric rather than magnetic heating predominated.

1 Introduction

Magnetic fluid hyperthermia (*MFH*) is a promising non-invasive and with minimal side effects medical therapy to treat human cancers, which makes use of magnetic nanoparticles (*MNPs*) that generate heat under alternating magnetic fields [1, 2]. Cancer hyperthermia therapies are based on the empirical principle that cancerous cells are more liable to high temperatures than healthy cells. If heat is properly distributed and kept an optimum time in the malignant tumor's body, such a tumor can be destroyed. A somewhat general and empirical prescription is to increase the tumor temperature at 43°C for 60 minutes to destroy such cancerous tumors [3]. Although there have been quite remarkable advances in establishing the *MFH* as a stand-alone methodology to treat cancers, there are yet several issues to be fully comprehended and controlled for safe clinical applications. One such an issue is to reach the desired temperature, say at 43°C in a minimum time and keep it for as long as it is needed.

Another issue connected with the latter is, to concentrate the heat in the tumor volume as much as possible, without affecting healthy tissues. To meet this goal another prescription is given, the *CEM43°C T90* (cumulative equivalent minutes at a standard targeted treatment temperature of 43°C obtained within 90 % of the tumor volume). A multiple treatment, say *10 CEM43°C T90* (10 treatments), is suggested to be a goal treatment [3].

On the other hand, to guarantee an effective heating at the treated site, i. e., the 90 % volume of the tumor, thermometry is required; thermometry in tumors is however, invasive and generates several complications [3]. Magnetic resonance imaging (*MRI*) as a non-invasive tool may solve this thermometry aspect [4] In parallel with *MRI* thermometry it is also required to know how to suffice in practice the *CEM 43°C T90* criterion. Several computational works have been carried out in the last two decades to get the best heating distribution conditions in phantoms, mimicking tumors. Parameters such as a critical concentration of

---

[1]   Instituto Nacional de Investigaciones Nucleares. Carretera México-Toluca s/n, La Marquesa, Ocoyoacac, Edo. de México, C. P. 52750, México

[2]   Centro Conjunto de Investigación en Química Sustentable, Universidad Autónoma del Estado de México, Campus UAEMéx "El Rosedal", km 14.5 Carretera Toluca-Atlacomulco, San Cayetano-Toluca de Lerdo, C.P. 50200, Estado de México, México

[3]   Facultad de Ciencias, Universidad Autónoma del Estado de México, Campus El Cerrillo, Carretera Toluca-Ixtlahuaca km 15.5, Piedras Blancas, 50200 Toluca de Lerdo, México

MNPs, their distribution and their residence time inside a tumor, the body regulating temperature system inside and outside the tumor and the operating parameters of the *MFH* system are all these taken into considerations in the mathematical simulations to reach the best heating conditions and make possible this cancer *MFH* treatment without producing any harm to the patient [2, 5].

Thus, contrary to any other cancer therapy, the *MFH* is practically non-invasive and can be applied in specific external and internal body points, since the heating *MNPs* can be injected practically in any part of the body or treating site.

Chronologically, the *MFH* has been tested in vitro and in vivo studies since the early 1990's systematically, with an exponential growing of published papers since then, as can be seen in Périgo et al.'s paper [6], where for example more than 400 papers were published in 2013 only. This line of research starts with the seminal paper of Gilchrist et al. in 1957 [7] who were the first to suggest this methodology to treat cancers. It was indeed until 1993 with the papers of Jordan et al. [8] and Chang et al. [9] that this methodology began to interest other researches.

Several research *MFH* systems are in current use, operating in different laboratories worldwide using frequencies between 50 and 13.56 MHz, and generating alternating magnetic fields from few hundred A/m to some hundred kA/m. The traditional set up of a laboratory *MFH* system is a copper coil connected to an LC resonant circuit which is connected to radiofrequency power amplifiers [10]. All these *MFH* systems privilege the magnetic over the electric properties of the heated media. However, because of the presence of conductive elements or dielectric materials that are present in the biologic and aqueous media, the electric heating is inevitable in these inductive systems.

Thus, the interest here is to discuss some *MFH* results while using an inductive system that operates at 13.56 MHz, providing a maximum magnetic field strength of $H_0 = 160$ A/m. *Escherichia coli* bacteria (*ECB*) and *mouse glioma* cells (*MGCs*) were exposed to this system in the presence of oleic acid coated and uncoated *MNPs* of magnetite/maghemite. Additionally, other aqueous and organic samples were included to study the heating sources in this inductive heating system.

2 Experimental

Concentrations from 1×10^3 to 1×10^6 FCU/mL of Gram negative *Escherichia coli* ATCC8739 and 1×10^6 to 3×10^6 of *MGCs* were used. Both microorganisms were prepared as reported elsewhere [11, 12]. Depending on sample type, up to four heating treatments were carried out simultaneously for both *ECB* and *MGCs*. Independently, two reference assays to measure the viability were carried out, one at 17°C, the laboratory room temperature (*LT*) and at 37°C, the human body temperature (*BT*). Whereas the thermal treatments for *ECB* ranged from 45°C to 50°C, for *MGCs* ranged from 40°C to 50°C, respectively. For comparative purposes, *ECB* or *MGCs* were treated simultaneously at the same temperature using direct heating in water (DH), ultrasound (*US*) and *MFH*. To test the cytotoxicity of the *MNPs* on these microorganisms, most thermal treatments were carried out in presence and absence of *MNPs*. Each treated sample was named according to its thermal mode treatment as follows: samples in absence of *MNPs* were named as *LTS, BTS, DHS, USS* and *MFS*; samples in presence of *MNPs* were named as *LTC, BTC, DHC, USC* and *MFC*. *MFS* and *MFC* refer to samples treated by using *MFH* in absence and presence of *MNPs*, respectively. From 7 to 15 mg/mL of *MNPs* were added to samples containing either the *ECB* or

MGCs. Depending on the experiment, the heating times ranged from 30 to 60 minutes. For this purpose, two types of experimental heating were carried out: (a) the continuous and (b) discontinuous heating modes. The first heating mode consisted on heating the samples continuously for 30 or 60 minutes time at the chosen temperature; the discontinuous heating mode consisted on heating the samples discontinuously for 10 minutes at the chosen temperature and then cooling them down at 37°C for 5 minutes. This discontinuous heating mode treatment was repeated three times to complete 30 cumulative minutes at the chosen temperature.

Uncoated and oleic acid coated *MNPs* based on magnetite/maghemite were, with mean particle sizes of 9.55, 8.5 and 5 nm, used. These *MNPs* were prepared by the reverse co-precipitation synthesis method [13].

The inductive heating system consisted on the 13.56 MHz radiofrequency generator Kurt J. Lesker, model R301, connected to a matching box, the *LC* circuit MMSeries. As load, a small copper coil was used. While operating this system at 250 W a magnetic field strength of $H_o = \pm 160$ A/m was obtained. Less than 2 % of fed energy was reflected from the resonant circuit. A Cole-Parmer laboratory ultrasound cleaner apparatus, model 08890-01 with output of 70 W and 47 kHz (± 6 %) was used.

2.1 *MNPs* characterization

The crystal structure and average particle size of some of the used *MNPs*, based on magnetite/maghemite, were characterized by X-ray diffraction (*XRD*) using the D5000 diffractometer coupled to a CuKαX-ray source from Siemens. The morphology, mean particle size and particle size distribution of these *MNPs* were analyzed by looking at the transmission electron microscopy (*TEM*) bright-field images. For this purpose was used a JEOL JEM-2100 model high-resolution *TEM*, operating at 200 kV. The iron oxidation state, the superparamagnetic, ferrimagnetic and the agglomeration state of the uncoated and oleic acid coated *MNPs* of Fe_3O_4/γ-Fe_2O_3 were analyzed by Mössbauer spectroscopy (MS). A Wissel Mössbauer spectrometer, calibrated with an iron foil 25 μm thick and operating in the constant acceleration mode was used. A radioactive source of ^{57}Co/Rh mounted in the transducer was used. Thus, the reported isomer shifts refer to that of metallic iron. A homemade least-squares fitting program was used to fit the resulting Mössbauer spectra.

3 Results and discussion

3.1 *XRD* and *TEM* analysis

Figure 1 shows the *XRD* patterns of uncoated and oleic acid coated magnetic samples. All indexed lines correspond to those indicated by the JCPDS no. 19-0629 card, which is consistent with the inverse spinel structure of Fe_3O_4 or γ-Fe_2O_3. The average crystal size, obtained as an average from the six Miller indexed line widths of each *XRD* pattern, using the Scherrer's equation, was 8.5 nm for uncoated magnetite sample, Fig. 1a, and 5 nm for oleic acid magnetite sample, Fig. 1b. These particle sizes were confirmed by analyzing the *TEM* bright-field images of these *MNPs* as observed from Fig. 2a and c, from which the particle size distribution (*psd*) was also measured, as depicted below their *TEM* images, showing the corresponding mean particle sizes of the used samples. As can be seen from the particle size distributions (*psds*), the presence of frail bimodal distributions are noted in Fig. 2a and b, an aspect that will be analyzed by Mössbauer spectroscopy. This bimodal aspect of the *psd* is less pronounced in the sample coated with oleic acid, Fig. 2c.
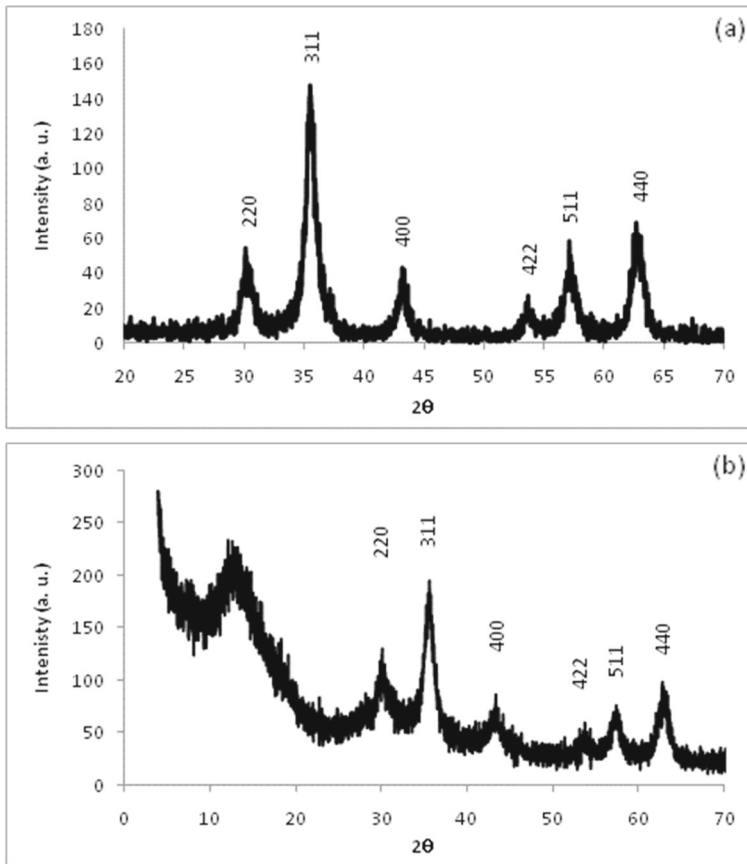
Fig. 1 XRD pattern of nanometric (**a**) uncoated and (**b**) oleic acid coated Fe_3O_4 particles

3.2 MS analysis

The room temperature Mössbauer spectra of the uncoated and oleic acid coated magnetites consisted of broad resonance spectra, as shown in Fig. 3. Whereas Fig. 3a and b show the Mössbauer spectra of uncoated samples with the bigger mean particle sizes of 9.5 and 8.5 nm, respectively, Fig. 3c shows the resulting Mössbauer spectrum of oleic acid coated sample with the smaller mean particle size of 5 nm. Mössbauer spectra of Fig. 3a and b show the typical smeared inward asymmetry of each line which is a characteristic spectral feature for inferring strong magnetic inter-particle interactions in nanomaterials [14, 15], or due to the presence of a bimodal *psd*, an aspect of interest for *MFH* experiments. The broad Mössbauer doublet appearing in Fig. 3c arising from the oleic acid coated sample can be associated with superparamagnetism due to the smallness of its mean particle size [14, 15]. It is interesting to observe the transmission properties of the uncoated and coated samples from Fig. 3. The coated sample presents a transmission effect of 9.5 % versus 2 and 4 % for the uncoated samples. Comparatively speaking, the coated sample would present the less magnetic inter-particle interaction (*mipi*) and therefore less particle agglomeration due to the presence of oleic acid at the particles surface [14].
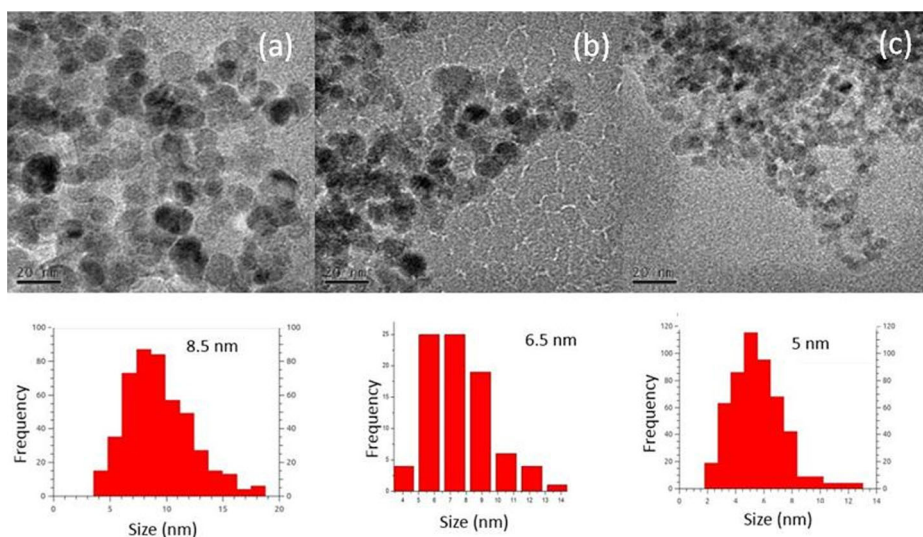
Fig. 2 TEM images as well as their frequency histograms with their mode size of pure magnetite **a**) 9.5 nm **b**) 8.5 nm and OA coated magnetite **c**) 5 nm

The relevant calculated data and fitted spectrum are also shown in Fig. 3 where two broad sextets characteristic of magnetite/maghemite are present in Fig. 3a and b. These sextets, with hyperfine magnetic fields of 46 and 41 T for Fig. 3a, and 47.5 and 44 T for Fig. 3b can be assigned to Fe^{3+} in A sites and Fe^{2+} and Fe^{3+} in B sites, respectively, located in the inverse spinel structure. One should note the slightly higher isomer shift values associated with the B sites (δ_B) which are 0.37 and 0.42 mm/s for Fig. 3a and b, respectively. Both these values are higher than the isomer shifts associated with the A sites, (δ_A), which is the same value for both samples of Fig. 3a and b, $\delta_A = 0.33$ mm/s. The resulting ratio $\delta_B/\delta_A > 1$ may be indicative of the presence of magnetite rather than pure maghemite. Low values of δ_B or close to those of δ_A may be due to two possibilities: (a) the magnetite is partially oxidized into maghemite and (b) the magnetite possess a very small particle size as discussed in [13]; both possibilities may also contribute as it would be in the present case. Additionally, and assuming the same Mössbauer fractions for A and B sites the resulting area ratios of these patterns of Fig. 3a and b are 1.18 and 2, and may also suggest that sample of Fig. 3a is practically maghemite, but for sample of Fig. 3b should be practically pure magnetite.

On the other hand, the quadrupole doublet shown in Fig. 3a may be associated with superparamagnetic particles or paramagnetic impurities [14]. One should also note that the line widths of both Mössbauer sextets associated with A and B sites of Fig. 3a and b are quite broad, relative to the natural Mössbauer line width (0.19 mm/s). These broad lines may be taken as a consequence of the presence of the *MNPs* having their own *psd*, and therefore generating a characteristic hyperfine field distribution (*hfd*). Since this line broadening is also the result of the *mipi* the resulting *hfd* arises from two contributions, the *psd* and the *mipi*. The separation of both these contributions to the *hfd* may result, if not impossible, quite a task. Thus in order to simplify this problem, the third broader sextet appearing in Fig. 3b, with the hyperfine magnetic field of 38.2 T, with a relative spectral contribution of 53.3 %, could be a qualitative measure of the *mipi*, i. e., the 53.3 % of the *MNPs*
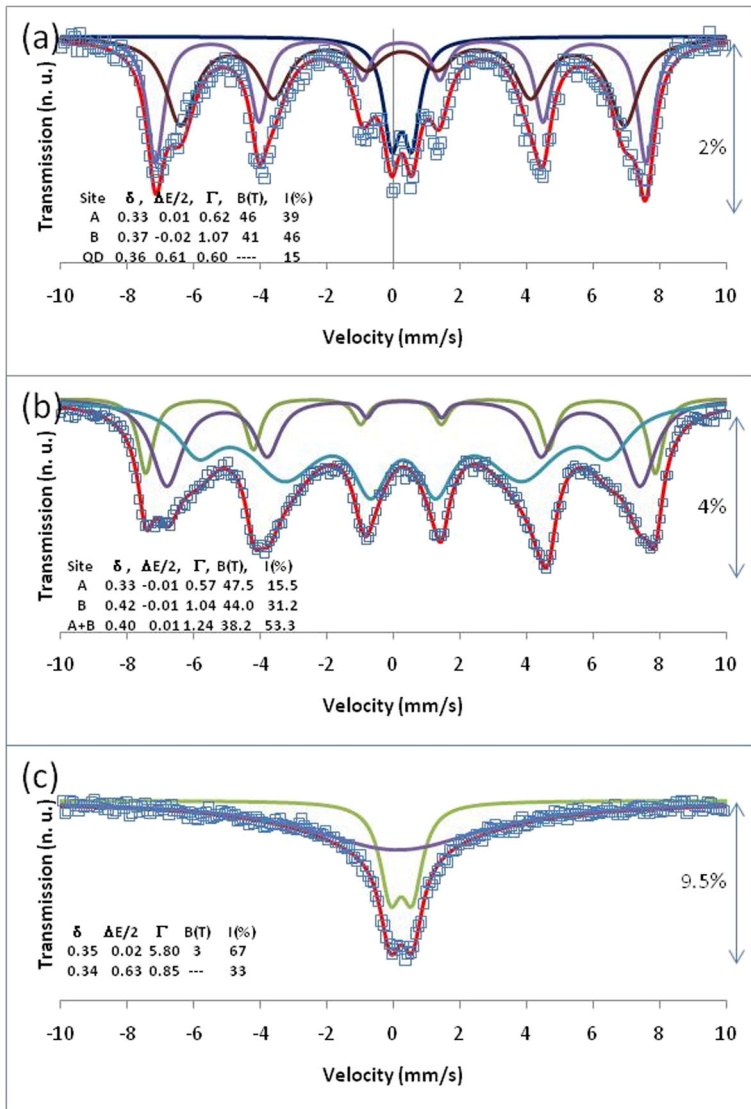
Fig. 3 Mössbauer spectra of pure magnetite with mean particle sizes of (**a**) 9.5 nm and (**b**) 8.5 nm, and oleic acid coated magnetite of mean particle size of (**c**) 5 nm

of magnetite are possibly agglomerated presenting *mipi*. Such an effect would be less pronounced in Fig. 3a where a third sextet was not required. A similar reasoning could be used in Fig. 3c where the fitted broad line having a small hyperfine magnetic field of only 3T, with a relative spectral contribution of 67 %, would arise from *mipi*. It is well known that well dispersed *MNPs* of Fe_3O_4 having mean particle sizes as small as 5, 8.5 or 9.5 nm, should show typical superparamagnetism which is not observed here [14]. All these samples had blocking temperatures that range from 200K to 250K [13]. Thus, one would expect agglomerated particles with sizes bigger than those measured by XRD or TEM images due

to a strong *mipi*. Thus, one could suggest from this analysis that the fitted quadrupole doublets, shown in Fig. 3a and c, would arise from relatively well dispersed superparamagnetic *MNPs*. In this sense, the uncoated *MNPs* of magnetite, presenting the intermediate mean particle sizes, would be quite agglomerated, which from the MFH standing point of view are less effective to generate heat by the Brownian relaxation mechanism [1, 6] and in this case by particle size considerations as explained later on. The nature of sample of Fig. 3c was pure maghemite as elucidated by low temperature Mössbauer measurements [13].

3.3 Hyperthermia results

3.3.1 ECB

Different tests were conducted with the objective of measuring the temperature dependence on the viability of the *ECB*. For these measurements oleic acid coated *MNPs* of maghemite were used. Figures 4 and 5 resume representative results after trying out different temperatures and heating times to kill the *ECB*. It can be observed from Fig. 4 that when the *ECB* was continuously heated at 45°C for 30 minutes the viability of the bacteria was relatively high for all media tested, i. e., the *DHS*, *DHC* and *MFC* heating modes. The highest viability was measured for the *MFC* treatment with 90 % survival. The viability of *ECB* for continuous heating at 50°C for 30 and 60 minutes is shown in Fig. 4b. The viability was in this case 32, 36 and 16 % for *DHS*, *DHC* and *MFC* heating modes, respectively, using the continuous heating mode for 30 minutes. These percentages decreased for the continuous 60 minutes treatment, where a total killing (*TK*) of the *ECB* in the *DHS* sample occurred only. A 16 % and 4 % survival were obtained for *DHC* and *MFC* treatments, respectively; form these results, the *MNPs* seemed not to show a cytotoxic effect. At this point, the direct heating in water at 50°C/60 minutes, in absence of *MNPs*, seemed to be a more effective treatment to kill the *ECB* than the *MFH* treatment in presence of *MNPs*.

Nevertheless, when the *ECB* was thermally treated in the discontinuous heating mode at 50°C by thrice and using 30 cumulative minutes only, as shown in Fig. 4c, the *MFC* treatment resulted to be systematically more effective to kill the *ECB* than any treatment, either *by DHS or DHC*. In such a discontinuous heating mode, the *ECB* survival was 12, 4 and 0.06 % for *DHS*, *DHC* and *MFC*, respectively. Now, the killing effect of the *MNPs* on the *ECB* seemed to be more effective than in the continuous heating mode, Fig. 4a and b, without discarding, in this case, a possible cytotoxic effect of the *MNPs*.

In Fig. 4a, *PAT* sample data represents the control number of forming colony units (*FCU*) of *ECB* at the moment of the preparation which did not differ much from the number left of *FCU* of *ECB* after exposing it to laboratory temperature (LT) conditions in absence of *MNPs* (sample *LTS*), during experiments. Thus *PAT* data will mostly be omitted in what follows unless otherwise stated, and our main reference data will be *LTS* sample data. In some few cases the reference data will also be *LTC* samples.

Figure 5.a, shows on the other hand, the comparative results of exposing *ECB* at 48°C, and 50°C thermal heating treatments in discontinuous mode by thrice. The viability of *ECB* at 48°C was 8, 48, and 8 % for *DHS, DHC* and *MFC*, respectively. A high survival was measured in *DHC* suggesting none cytotoxic effect of the *MNPs*. It can also be observed from Fig. 5a, that the viability of *ECB* at 50°C, as already described, was practically null (a 0.06 % survival) in the *MFC* heating mode, which was a systematic result at this temperature. On the other hand, the viability of *ECB* at 50°C in *DHC* was in this case, lower than in *DHS*, opposite to the 48°C case, making difficult to assess a toxic effect of the *MNPs* on *ECB* considering these results only.
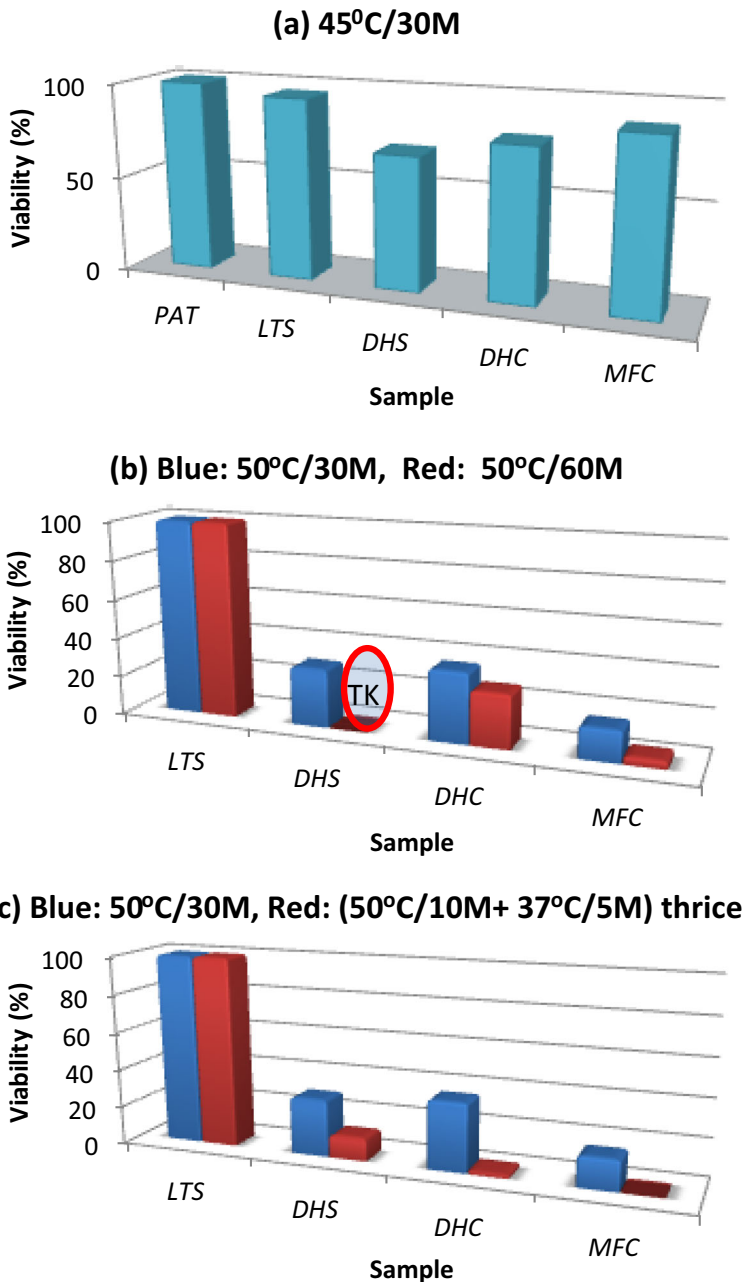
(a) 45⁰C/30M

(b) Blue: 50ºC/30M, Red: 50ºC/60M

(c) Blue: 50ºC/30M, Red: (50ºC/10M+ 37ºC/5M) thrice

Fig. 4 Viability of ECB heated at (**a**) 45°C for 30 minutes time continuously and (**b**) 50°C for 30 and 50 minutes times continuously and at (**b**) 50°C in discontinuous heating mode by thirce

Figure 5b shows the 48°C treatment by thrice including the *PAT* reference data, and *USC* and *MFS* and *MFC* treatments. Firstly, as observed from this figure, the viability of *ECB* for the *MFS* sample did not change much from that of the *MFC* sample. The percentages were
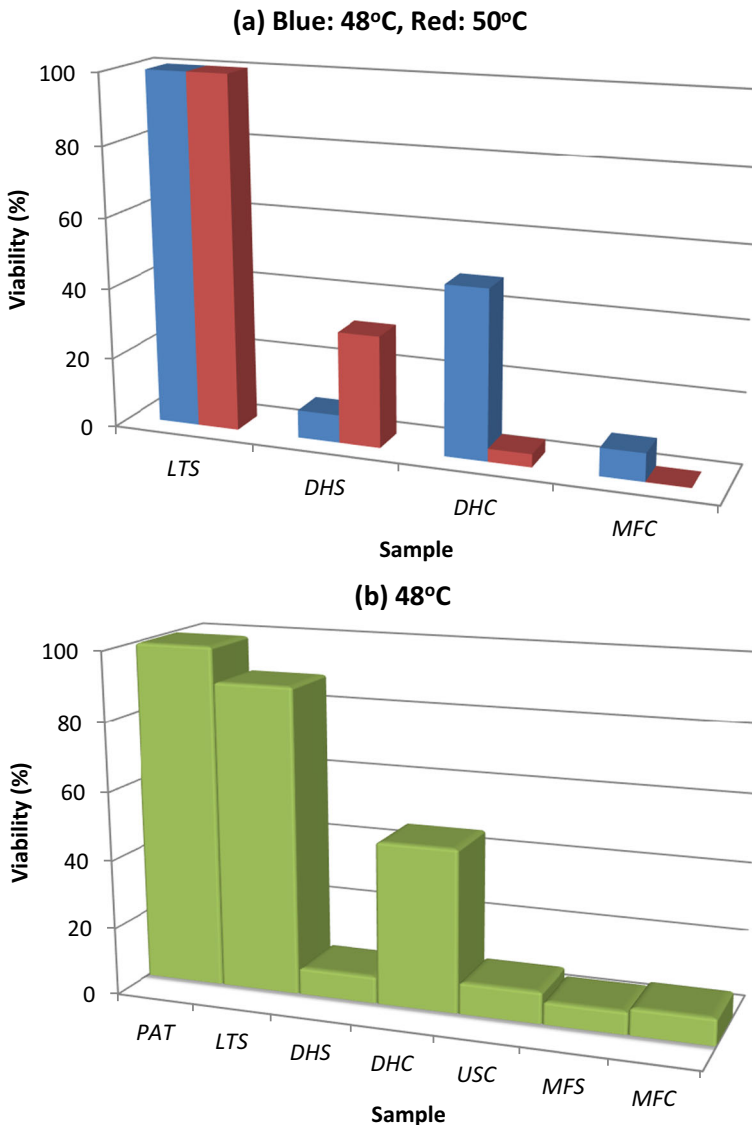
Fig. 5 *ECB* viability at (**a**) 48°C and 50°C in paused heating modes by thrice, and (**b**) at 48°C by paused heating mode by thrice, including ultrasound in presence of MNPs (USC) and the inductive heating mode in absence of MNPs (MFS) treatments

6.6 and 7.9 % for *MHS* and *MFC*, respectively, i. e., by considering an experimental error of $\sim \pm 2$ %, these values represent the same viability. Secondly, ultrasound (US) treatments results to be an effective mean to destroy these microorganisms, either by ultrasound shock waves [17] or cavitation [this work]. The viability of *ECB* in *USC* was relatively low and just above that of *MHS* or *MHC* samples with a viability of 9.3 %. By including these results one then may suggest that the *MNPs* do not have any toxic effect on *ECB*. That is, whereas the 50°C treatment, Fig. 4, may suggest a toxic effect of the *MNPs* on *ECB*, those
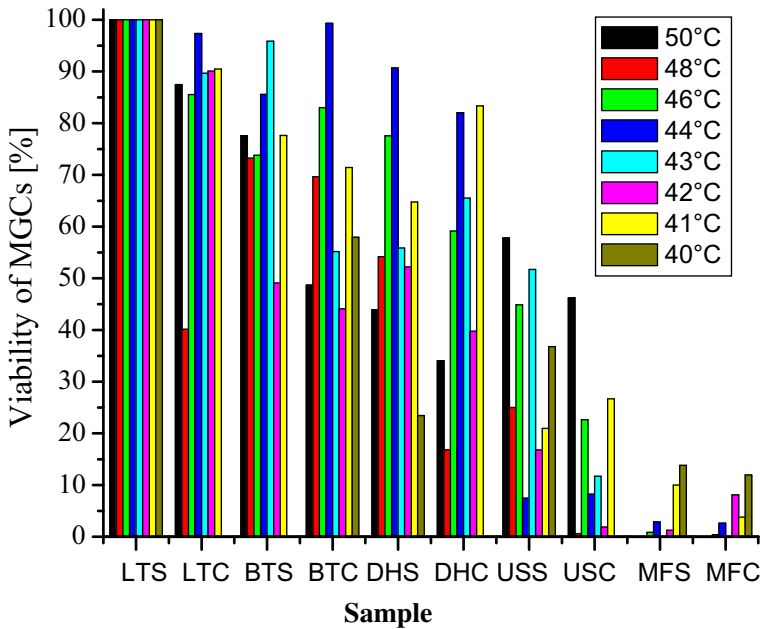
Fig. 6 *MGCs* viability from 40°C to 50°C using the discontinuous heating mode by thrice

treatments at 45°C and 48°C, either in the continuous or discontinuous heating modes, this effect may be discarded. One should add a final comment related to the toxic effect of the *MNPs* since the concentrations used here were relatively large, thus one would expect that by using biomedical concentrations of ppm, such a toxic effect would be practically reduced or eliminated.

3.3.2 MGCs

Figure 6 also resumes all pertinent experiments on the *MGCs* viability, treated from 40°C to 50°C, using the discontinuous heating mode only. Generally speaking, the *MGCs* viability decreases as the temperature increases, as in the *ECB* case occurred. The viability presented, however, some important particularities.

A closer look at particular temperatures is discussed next. The 48°C and 50°C treatments are shown in Fig. 7a and b where the *MGCs* viability was null for *USS*, *USC, MFS* and *MFC* samples. As in the preceding case, the direct heating in water, either in presence or absence of *MNPs*, was always less effective to kill *ECB* than either *US* or *MFH*. Particularly, for samples *DHS* and *DHC* the viability of *MGCs* at 50°C was higher than at 48°C, see Fig. 7a and b. Below these temperatures the viability of *MGCs* was sometimes higher than zero for *US* and *MFH*, as can be seen in Fig. 6. Figure 7c shows, on the other hand, the *MGCs* viability at 49°C for 30 minutes in the continuous heating mode, in which the viability was higher than zero for all samples, including those of *MFC* and under *USC* and *USS* conditions.

There was, on the other hand, an interesting result while treating the *MGCs* under ultrasound. For instance, after treating the *MGCs* at 40°C and 48°C there were any signs of alive and death cells, only tiny traces of cellular material, i.e., the cells were totally destroyed (*TD*). Though we did not look at the precise conditions to get always this type of results,
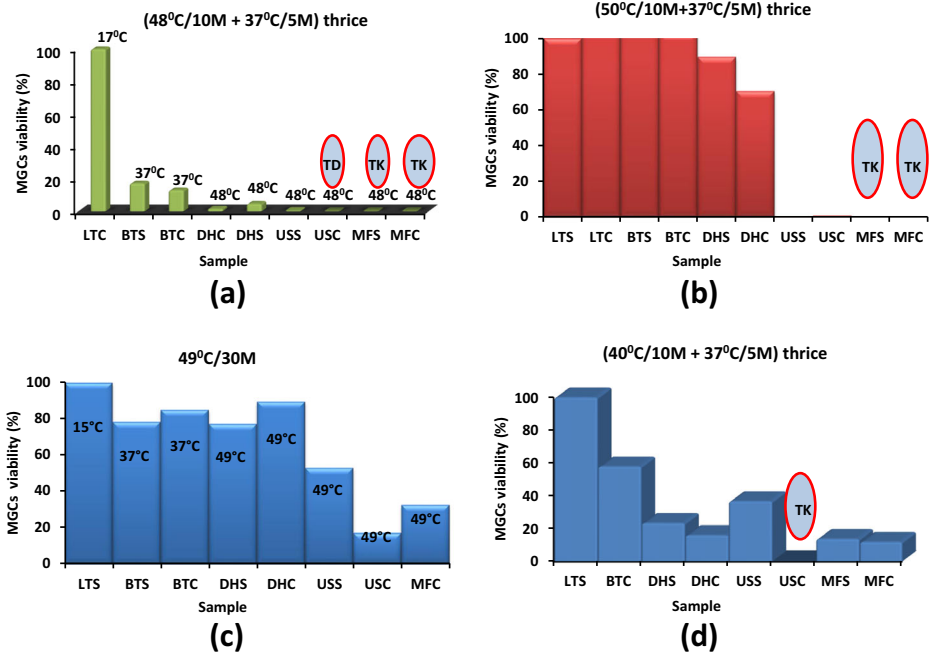
Fig. 7 *MGCs* viability at (**a**) 48°C and (**b**) 50°C, in discontinuous heating mode, at (**c**) 49°C for 30 minutes in continuous heating mode and at (**d**) 40°C in discontinuous heated mode, respectively. At the top of each bar in figure (**a**) appears the corresponding temperatures

which was outside of the objective of this work, it is important to point out that this total cell destruction occurred at as low as 40°C as shown in Fig. 7d. The same occurred at 46°C where in both the *USS* and *USC* treated samples the *MGCs* were totally destroyed.

It is of particular interest to show the viability of *MGCs* between 42 and 44°C, the temperature interval where cancerous cells begin be more liable than healthy cells.

Figure 8 shows the viability of *MGCs* under different heating treatments using the percent and $\log_{10}$ data presentations. For instance, the viability of *MGCs* at 42°C (Fig. 8a) may appear to be low enough for *USC* and *MFS* if the percent data are reported. This is, however, not as low as one may think, Fig. 8b, shows the $\log_{10}$ data for *MGCs* survival in *US* and *MFH* media which is of the order of 10^4 and 10^5 cells/mL. On the other hand, the treatment at 43°C resulted in total killing (TK) in both the *MFS* and *MFC* media, as shown in Fig. 8c; this result was, however, not reproducible. For *DH* and *US* treatments the viability at 43°C was relatively high as shown in Fig. 8d. The viability of *MGCs* at 44°C, Fig. 8e and f, on the other hand, showed to be somewhat like that at 42°C, i. e., $\sim 10^4$ cells/mL survived for *US* and *MFH* treatments. In all cases studied, the viability of *MGCs* in the *DH* modes were, however, always higher than for the *US* and *MFH* treatments. So it is required to look for other heat protocols to reduce the viability of cancerous cells.

Thus from present in vitro results, it is shown that the *MGCs* may require temperatures higher than the targeted 43°C to destroy them systematically, under the present experimental conditions, and as described earlier in the introduction section. Though *US* treatments showed interesting results, the *MFH* treatments resulted to be more systematic and effective to kill these microorganisms than either *DH* or *US* treatments.
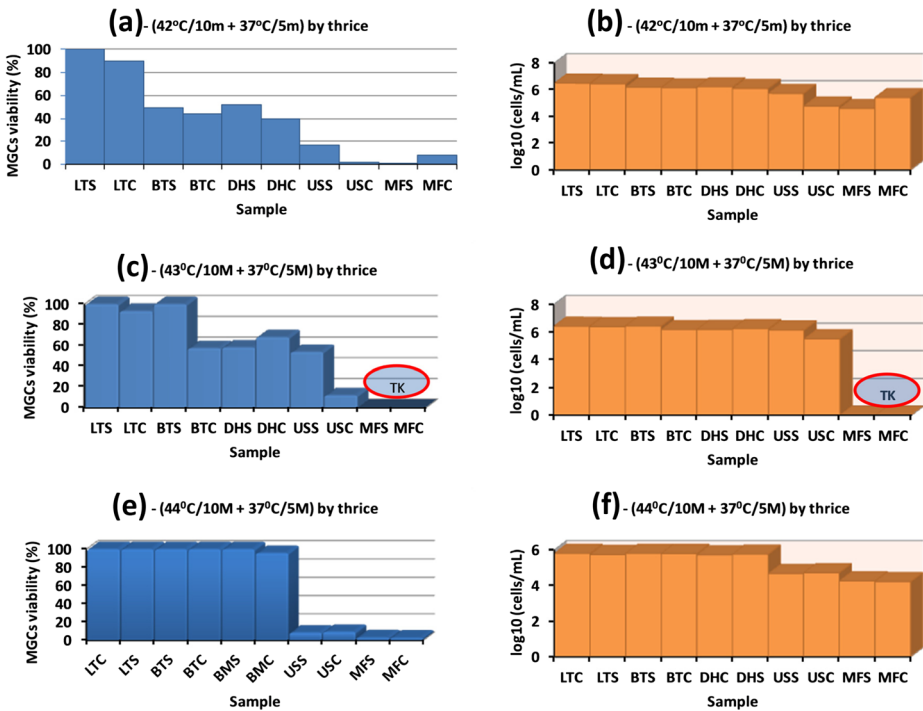
Fig. 8 *MGCs* treated at (**a**, **b**) 42°C, (**c**, **d**) 43°C and (**e**, **f**) 44°C

3.4 Heating features of the *MFH* system

It is worth mentioning the following comments in relation to the effect of *MNPs* under the *MFH* system. As observed from Figs. 5, 7a, b, and c, the *MGCs* viability under the inductive heating system (*MFH*) with and without *MNPs* appear to be approximately the same. A detailed analysis of this ambiguity was made. For instance, Fig. 9 shows theoretical plots of the power dissipation density (P) as a function of mono size dispersed particles of magnetite, and as a function of radiofrequencies of 100, 200, 300 kHz and 13.56 MHz. For generating Fig. 9a the data of Rosensweig's paper were used [1] plus the radiofrequency (RF) of our system, $f = 13.56$ MHz. For generating Fig. 9b, our operations conditions, $f = 13.56$ *MHz and* $H_0 = 160$ A/m, were used. Firstly, one can observe from Fig. 9a that the optimum size of the *MNPs* of magnetite to generate heat, magnetically and efficiently, decreases as the RF increases, thus our system requires nano-particles with diameter of ~ 15 nm. Our *MNPs* had, in this case, diameters <10 nm, suggesting that they are quite inefficient to generate heat by magnetic means. Secondly, plots in Fig. 9a were generated by using a magnetic field strength of $H_0 = 40$ kA/m. One can also observe from Fig. 9a that as the frequency increases, the maxima of P also increases. As a matter of fact the peak maximum of the plot generated with $f = 13.56$ MHz was divided by a factor of 30 to have a good view of the whole plots. Thirdly, Fig. 9b shows that maximum power loss density by using the parameters of our inductive system, $f = 13.56$ MHz and $H_0 = 160$ A/m, being much lower by a factor of about 2×10^4.
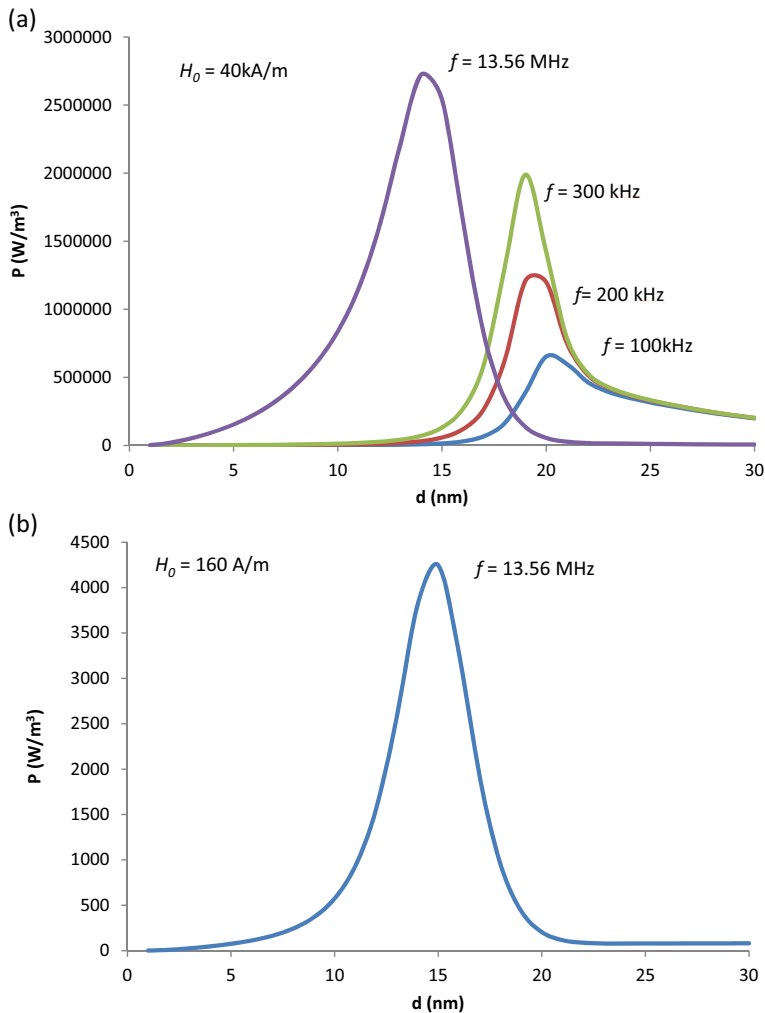
(a)

(b)

Fig. 9 The power loss dissipation, P, is plotted as a function of the particle size diameter of magnetite and as a function of radiofrequency. (**a**) In order to generate these plots a H0 = 40kA/m was used; the rest of the data for magnetite were taken from [1]. (**b**) To generate this plot H0 = 160 A/m, the maximum magnetic field strength obtained from our magnetic inductive system

Because our *MNPs* did not contribute as a magnetic heating source, different substances were thus used to investigate the origin of the generated heat of our system. The first samples tested were cyclohexane, glycerin and deionized water having the lowest (2), intermediated (23) and higher (80) dielectric constants, respectively. As expected the lowest generated heat was obtained while using cyclohexane with a $\Delta T_{cyclohexane} = 3.3°C$, followed by glycerin with a $\Delta T_{glycerin} = 15°C$. Interestingly the generated heat of deionized water was just above that of cyclohexane with $\Delta T_{deionized\ water} = 5°C$. This suggests that the generated heat by glycerin must be associated with another property different from the dielectric one. In order to test the heating properties of the *MNPs* of magnetite with a mean particle size of 8.5 nm [11], these were dispersed in cyclohexane. As seen from Fig. 10 the heating
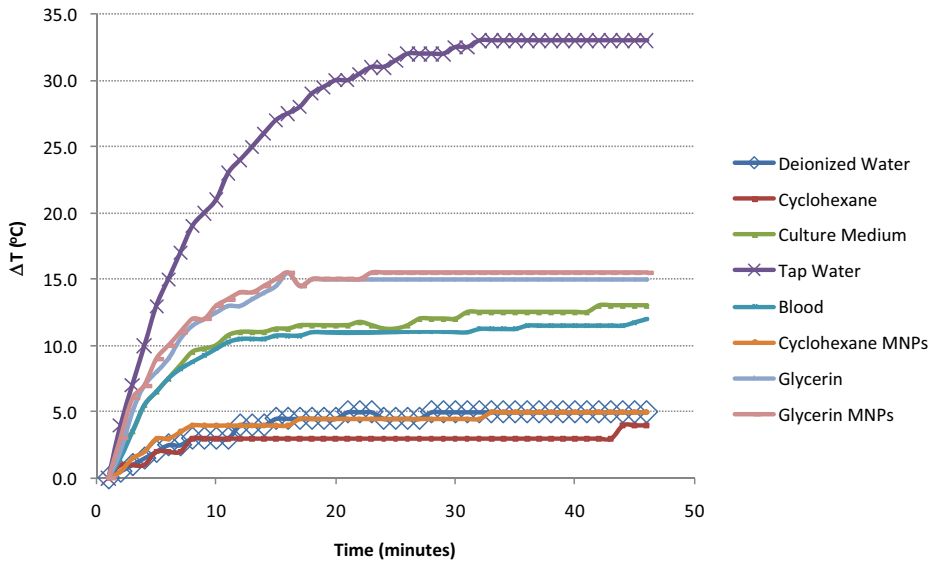
Fig. 10 Heating properties of the inductive system used, under aqueous and nonaqueous media, in presence and absence of *MNPs*

properties of these *MNPs* is minimum, getting a $\Delta T_{MNPS} = 1.7°C$ a value that results from the difference between $\Delta T_{cyclohexane+MNPS} - \Delta T_{cyclohexane} = 5°C - 3.3°C = 1.7°C$. This low heating effect of the *MNPs* can also be seen in the sample glycerin+*MNPs* with a $\Delta T_{MNPs} = 0.5°C$ as obtained from $\Delta T_{glycerin+MNPS} - \Delta T_{glycerin} = 15.5°C - 15°C = 0.5°C$. It can also be seen from Fig. 10 that tap water was the sample that generated more heat than any other sample tested, with a $\Delta T_{tap\ water} = 33°C$. Such a capacity to generate heat under the present inductive system must be associated with the salts content and other impurities like chlorine, an aspect that will be further studied in the near future. To give an idea of the complexity of the problem that results from tap water, isotonic water with 0.9 % of *NaCl* produces a $\Delta T = 4°C$ only.

The two remaining samples analyzed, as shown in Fig. 10, are the cellular culture medium and human blood, the former giving a $\Delta T_{cellular\ culture\ medium} = 13°C$ and human blood just below it with $\Delta T_{human\ blood} = 12°C$. One must deduce from present data that the properties of organic material either from the cellular culture medium and human blood or those involved in *ECB* and *MGCs* play a significant role in the heating characteristics of this inductive heating system.

This aspect parallels the observed in the capacitive heating system while trying to discern the heating properties of gold nanoparticles (*GNPs*) in presence of cancerous cells, where the produced heating is finally associated with the impurities of the samples, an aspect that has not been clearly elucidated yet [14].

4 Conclusions

In the present work the ***E. coli*** bacteria and mouse glioma cells were thermally treated by different means to elucidate their thermal resistance. ***E. coli*** bacteria and mouse glioma

cells under the *MFH* treatments only did not support temperatures higher than 50°C and 48°C, respectively. At these temperatures and above they were killed completely. When *MGCs* were exposed to ultrasound, the cells were completely destroyed at 40°C, 46°C and 48°C; for these cases none sign of cell structures or organic material was observed under the optic microscope. Thus, present results suggest that higher temperature than 40°C may not be required to kill cancerous cells while using ultrasound of low frequency. Present results also showed that in our inductive system magnetic heating did not occur due mainly to the suspended nature of the magnetite particles and because of their low mean particle size diameter; instead, this heating was entirely due to the electric properties of aqueous and/or biological samples and was sufficient to kill either the *E. coli* bacteria or the mouse glioma cells.

References

1. Rosensweig, R.E.: Heating magnetic fluid with alternating magnetic field. J. Magn. Magn. Mater. **252**(2002), 370–374 (2002)
2. Adhikary, K., Banerjee, J.: A thermofluid analysis of the magnetic nanoparticles enhanced heating effects in tissues embedded with large blood vessel during magnetic fluid hyperthermia. J. Nanopart. **2016**, 18. Article ID 6309231 (2016). doi:10.1155/2016/6309231
3. Chichel, A., Skowronek, J., Kubaszewska, M., Kanikowski, M.: Hyperthermia – description of a method and a review of clinical applications. Rep. Pract. Oncol Radiother **12**(5), 267–275 (2007)
4. Gellermann, J., Hildebrandt, B., Issels, R., Ganter, H., Lodarczyk, W., Budach, V., Felix, R., Tunn, P.U., Reichardt, P., Wust, P.: Noninvasive magnetic resonance thermography of soft tissue sarcomas during regional hyperthermia. Correlation with response and direct thermometry. Cancer **107–6**, 1374–1382 (2006)
5. Nabil, M., Decuzzi, P., Zunino, P.: Modelling mass and heat transfer in nano-based cancer hyperthermia. R Soc Open Sci **2**, 150447 (2015)
6. Périgo, E.A., Hemery, G., Sandre, O., Ortega, D., Garaio, E., Plazaola, F., Teran, F.J.: Fundamentals and advances in magnetic hyperthermia. Appl. Phys. Rev. **2**, 041302 (2015). doi:10.1063/1.4935688
7. Gilcrist, R.K., Medal, B., Shorey, W.D., Hanselman, R.C., Pamotrr, J.C., Bruce Taylor, C.: Selective inductive heating of lymph nodes. Annals Surg. 596–606 (1957)
8. Jordan, A., Wust, P., Fähling, H., Johns, W., Hinzt, A., Felix, R.: Inductive heating of ferrimagnetic particles and magnetic fluids: Physical evaluation of their potential for hyperthermia. Int. J. Hyperth. **9**, 51–68 (1993)
9. Chan, D.C.F., Kirpotin, D.B., Bunn Jr., P.A.: Synthesis and evaluation of colloidal magnetic iron oxides for the site-specific radiofrequency-induced hyperthermia of cancer. J. Magn. Magn. Mater. **122**, 374–378 (1993)
10. Lacroix, L.M., Carrey, J., Respaud, M.: A frequency-adjustable electromagnet for hyperthermia measurements on magnetic nanoparticles. Rev. Sci. Instrum. **79**, 093909 (2008)
11. Gutiérrez-León, D.G., Rodríguez-Méndez, B.G., López-Callejas, R., Peña-Eguiluz, R., Valencia-Alvarado, R., Mercado-Cabrera, A., Muñoz-Castro, A.E., Belman-Flores, J.M. Experimental evaluation of DBD reactor applied to bacterial inactivation in water flowing continuously. IEEE Trans. Plasma Sci. (2016). doi:10.1109/TPS.2016.2572640
12. Perez, A., Santos-Cuevas, C.L., Chairez, I., Poznyak, T., Ordaz-Rosado, D., García-becerra, R., Romero Piña, M.E.: Ozone dosage effect on C6 cell growth: in vitro and in vivo tests. Anti-Cancer Agents in Medicinal Chemistry (Formerly Current Medicinal Chemistry-Anti-Cancer Agents) **15**(9), 1190–1196 (2015)
13. Almazán Celis, J., Olea Mejía, O.F., Cabral Prieto, A., García-Sosa, I., Escudero Derat, R., Baggio Saitovitch, E.M., Alzamora Camarena, M.: This paper form part of the proceedings of LACAME 2016, Taaken place in Panamá November 2016 (2016). doi:10.1007/s10751-017-1414-x

14. Mørup, S., Hansen, M.F., Frandsen, C.: Magnetic interactions between nanoparticles. Beilstein J. Nanotechnol. **1**, 182–190 (2010)
15. Brok, E., Frandsen, C., Madsen, D.E., Jacobsen, H., Birk, J.O., Lefmann, K., Bendix, J., Pedersen, K.S., Boothroyd, C.B., Berhe, A.A., Simeoni, G.G., Mørup, S.: Magnetic properties of ultra-small goethite nanoparticles. J. Phys. D. Appl. Phys. **47(36)**, 13. Article ID 365003 (2014). doi:10.1088/0022-3727/47/36/365003
16. Liu, X.: Exploration of the Interaction of Electromagnetic Fields with Nanoscale Materials. Doctoral thesis, School of Electronic Engineering and Computer Science Queen Mary University of London (2012). http://qmro.qmul.ac.uk/jspui/handle/123456789/8559
17. Müller, P., Guggenheim, B., Attin, T., Marlinghaus, E., Schmidlin, P.R.: Potential of shock waves to remove calculus and biofilm. Clinical Oral Investigations **15**(6), 959–965 (2011)